STUDIES ON NUCLEATION PROCESS IN DIAMOND CVD: AN OVERVIEW OF RECENT DEVELOPMENT

Huimin Liu and David S. Dandy
Department of Chemical Engineering, Colorado State University, Fort Collins, CO 80523

Abstract

This paper presents an updated and systematic overview of the recent development in studies on nucleation process in diamond CVD. The nucleation mechanisms are discussed, and the nucleation enhancement methods developed to date are summarized. The effects of surface conditions and deposition parameters on the surface nucleation are described. Finally, a brief description of theoretical and modeling studies on the surface nucleation is given.

1. Introduction

Over the past 40 years a variety of techniques have evolved for the synthesis of diamond, including High Pressure High Temperature (HPHT) processes, Chemical Vapor Deposition (CVD), and Physical Vapor Deposition (PVD). The CVD process, one of the most important technological developments in the past decade, makes production of high-quality diamond coatings on preshaped parts and synthesis of free-standing shapes of diamond a reality. Epitaxial diamond has been grown on diamond and cBN. Polycrystalline diamond films have been deposited on various non-diamond substrates, including insulators, semiconductors and metals, ranging from single crystals to amorphous materials. The success in growing diamond thin films using CVD methods has stimulated enormous interest in the unique properties of diamond for new technological applications. The combined properties of good electrical insulation, high thermal conductivity, and low dielectric constant make diamond well suited for use in device packaging and multichip module technologies; the extreme hardness and wide optical band gap provide an excellent material for a variety of optical applications; and the chemical inertness along with the high hardness makes diamond thin films an ideal protective coating against corrosion and wear in cutting tool and metal working industries.

The potential for economic scale-up of diamond CVD qualifies it as a viable processing alternative to HPHT for production of diamond abrasives or heat sinks at a cost that is still high but will be reduced as the technology improves. Moreover, CVD processes offer an opportunity to exploit many desirable physical properties of diamond (Table 1). The ability to coat a large area on a variety of substrate materials with CVD diamond films vastly expands the potential application areas of diamond over those possible with natural or HPHT-synthetic diamond. This capability, along with the need to explain the improbable growth of diamond under apparently

metastable conditions, has stimulated active research into all aspects of diamond CVD in all the major industrialized countries over the world. As potential applications of CVD diamond are continuously discovered, it may be anticipated that the ultimate economic impact of this emerging technology on the defense, space, and commercial areas will outstrip that of high-temperature superconductors with more immediate applications [1].

Table 1. Properties of CVD diamond and single-crystal diamond [2]

	CVD diamond	Single-crystal diamond
Density (g cm^{-3})	2.8–3.51 [1]	3.515
Thermal capacity at 27 ˚C (J $mol^{-1}K^{-1}$)	6.12	6.195
Standard entropy at 27 ˚C (J mol^{-1} K^{-1})		2.428
Standard enthalpy of formation at 27 ˚C (J mol^{-1})		1.884
Effective Debye temperature at 0 – 827 ˚C, (K)		1860 ± 10
Thermal conductivity at 25 ˚C * (W $m^{-1}K^{-1}$)	2100****	2200
Thermal expansion coefficient at 25–200 ˚C** ($\times 10^{-6}$ $˚C^{-1}$)	~2.0 [2, 3]	0.8–1.2 [2, 3]
Band gap (eV)	5.45	5.45
Electrical resistivity (Ω cm)	10^{12}–10^{16}	10^{16}
Dielectric constant at 45 MHz – 20 GHz	5.6	5.7
Dielectric strength (V cm^{-1})	10^6	10^6
Loss tangent at 45 MHz – 20 GHz	< 0.0001	
Saturated electron velocity ($\times 10^7$ cm s^{-1})	2.7	2.7
Carrier mobility (cm^2 V^{-1} s^{-1}) electron (n) positive hole (p)	 1350–1500 480	 2200 1600
Young's modulus * (GPa)	820–900*** at 0–800 ˚C [4]	910–1250
Compression strength (GPa)		8.68–16.53
Poisson's ratio		0.10–0.16
Coefficient of friction in air	0.035–0.3 [5]	0.05–0.15
Vickers hardness * (GPa) [varies with crystal orientation]	50–100	57–104
Index of refraction at 10 μm	2.34–2.42	2.40

* higher than any other known materials

** lower than Invar

*** *Young's modulus=895{1–1.04*$\times 10^{-4}$(T–20)}, (GPa), where T in ˚C [6].

**** Anisotropic characteristic of thermal conductivity of a thick CVD diamond film may be found in [7].

However, numerous earlier attempts to grow diamond films on non-diamond substrates have yielded only polycrystalline films consisting of randomly oriented crystals and containing a varying amount of non-diamond carbon and defects. In most CVD methods, diamond nucleation on non-diamond surfaces without pretreatment is usually very difficult and slow. Most earlier studies on the low pressure CVD of crystalline diamond have focused on examining various deposition techniques and characterizing the deposited films. These studies have led to a reasonable understanding of growth mechanisms and processing parameters. Recently, extensive work [8-25] on the nucleation and early growth stages has been performed in an effort to enhance diamond nucleation and to control film morphology. As a result, technology problems associated

with the nucleation of polycrystalline diamond films have been adequately addressed. A number of nucleation enhancement methods [26-38] have been developed that enable the control of nucleation density over several orders of magnitude. Nucleation density has been increased from $<10^5$ cm^{-2} on untreated substrates up to 10^{11} cm^{-2} on scratched or biased substrates [39,40]. The effects of surface conditions and deposition parameters on the nucleation process have been investigated [12,16,18,21,41-50] to provide the guideline for the selection of optimum surface pretreatment methods and deposition parameters. Recent advances in experimental measurement methods make it possible to directly observe the nucleation stage, and in some cases *in-situ* and/or *in vacuo* measurements [23,40]. The experimental investigations have significantly contributed to understanding of the nucleation mechanisms in diamond CVD. Progress has also been made in heteroepitaxial, highly oriented and textured growth [51]. Novel approaches [28,29] have evolved toward obtaining diamond films of a near-single-crystal morphology over large areas and may allow diamond to realize its potential as an electronic material in the near future.

It has become increasingly evident that further technological development in CVD of diamond films, particularly in such challenging areas as single-crystal growth for electronic applications and low-temperature deposition for coating on optic and plastic materials, requires a detailed understanding and an effective control of the fundamental phenomena associated with diamond nucleation and growth. These phenomena, especially the nucleation process, critically determine the film properties, morphology, homogeneity, defect formation, adhesion, and the type of substrates that can be successfully coated [22]. Therefore, the objective of the present paper is to overview the recent development in the nucleation studies in diamond CVD, in an attempt to provide insight into the fundamental phenomena associated with the nucleation process. The nucleation mechanisms will be discussed on the basis of the experimental observations, and the nucleation enhancement methods developed to date will be summarized. The effects of surface conditions and deposition parameters on the surface nucleation will be described. Finally, theoretical and modeling studies on the surface nucleation will be briefly reviewed.

2. Results and Discussion

2.1. Gas phase nucleation

Homogeneous nucleation in the gas phase and its contribution to different deposition processes are poorly understood. However, there is evidence that, at least in some cases, diamond can be nucleated homogeneously in the gas phase [52-54]. Derjaguin and Fedoseev [46] presented theoretical arguments, based on the classical nucleation theory, that homogeneous nucleation is possible. Matsumoto and Matsui [55] suggested that hydrocarbon cage molecules such as adamantane, bicyclooctane, tetracyclododecane, hexacyclopentadecane, and dodecahedrane are possible embryos for homogeneous nucleation of diamond. The adamantane molecule, $C_{10}H_{16}$, represents the smallest combination of carbon atoms which posses the

diamond unit structure, i.e., three six-member rings in a chair conformation. The tetracyclododecane and hexacyclopentadecane molecules represent twinned diamond embryos that were proposed as precursors to the fivefold twinned diamond microcrystals prevalent in CVD diamond films. From simple atomic structure comparison, one can easily generate the diamond lattice from these cage compounds by simple hydrogen abstraction followed by carbon addition. However, thermodynamic equilibrium calculations [56] revealed that such low molecular weight hydrocarbons are not stable at high temperatures (>600 ˚C) in the harsh environment associated with diamond CVD.

A limited number of experiments [52-54] have been conducted to examine homogeneous nucleation of diamond in the gas phase at atmospheric and subatmospheric pressures. The number of diamond particles collected from the gas phase is very small compared to typical nucleation densities observed on substrate surfaces. Therefore, the homogeneous nucleation mechanism cannot account for the large variety of nucleation densities observed on different substrate materials and from different surface pretreatments. It is speculated and also supported by a recent experiment [57] that the nuclei formed in the gas phase may reach the growing surface and increase the surface nucleation density. However, whether and how the diamond particles formed in the gas phase could serve as seeds on the substrate surface for subsequent growth of a diamond film remain unknown.

2.2. Surface nucleation

Frank-van der Merwe 2-D layer-by-layer growth [58] is the growth mode of diamond homoepitaxy and heteroepitaxy. Volmer-Weber 3-D island growth [58] is the mode of nucleation and growth of polycrystalline diamond films directly on non-diamond substrates due to the highest surface energies of diamond among any known materials (see Tables 3 and 4 below). A conventional growth process in CVD of polycrystalline diamond films typically shows several distinguishable stages [59]: (i) incubation period, (ii) 3-D surface nucleation, (iii) termination of nucleation and 3-D growth of nuclei to grains, (iv) coalescence of individual grains and formation of continuous film, and (v) growth of continuous film. Two criteria must be satisfied for 'spontaneous' (non-epitaxial) surface nucleation [33,60]: (a) carbon saturation of the substrate surface, and (b) presence of high-energy sites (unsatisfied valences).

Diamond nucleation on non-diamond substrates is generally proposed to occur mostly on an intermediate layer of diamond-like amorphous carbon [9-11,30,35,61], metal carbides [12,14,16,22,23,25,28,29,40,62-70], or graphite [13,17,19,32,34,62,71] formed at the substrate surface due to chemical interactions between activated gas species and the surface during the incubation period. Such intermediate layers provide nucleation sites for diamond crystallite growth [9,17,70], and hence enhance diamond nucleation densities on non-diamond substrates [21,37,70,71] and offer an opportunity for controlling the morphology [21,37], orientation and

texture [28,29] of diamond films. The thickness of the interlayers ranges from several angstroms (6 Å graphite on Pt [17]), to nanometers (8 nm graphite on Ni [17]; 8–14 nm DLC on Cu [9]; 20 nm a-C on Si [61]; 1–10 nm SiC on Si [40,65,67,69]), up to a few micrometers (1.5–3 μm Mo_2C on Mo [16,69]). The representative nucleation mechanisms proposed in published literature are summarized in Figures 1-3 [9,13,72].

Nucleation on an intermediate layer of diamond-like amorphous carbon

The HRTEM study of nucleation and growth of diamond on copper TEM grids in HFCVD by Singh [9] provided direct evidence for the formation of a diamond-like amorphous carbon layer, 8–14 nm thick, in which small diamond nanocrystallites approximately 2–5 nm across were embedded, and large diamond crystallites were observed to grow from these nanocrystallites. It was suggested [9] that the diamond nanocrystallines are formed as a result of direct transformation of the a-C into diamond, with the intermediate layer providing nucleation sites. Figure 1 depicts the detailed nucleation mechanism proposed on the basis of these experimental observations. In step I, carbon clusters are formed on the substrate surface and a change in the bonding structure from sp^1 to sp^2 takes place. In step II, sp^2 bonded carbon atoms are converted into relatively stable network of sp^3 bonded carbon. The continuous molecular rain of activated hydrocarbon and atomic hydrogen on the substrate surface provides sufficient energy for the sp^1 -> sp^2 -> sp^3 conversion. At the same time, etching of unstable phases (sp^1 and sp^2) which is ten times faster than etching of stable phase (sp^3) promotes and stabilizes the sp^3 phase. In step III, a transition of the bonding state in the carbon network occurs from a disordered domain with sp^3 bonded carbon to diamond with sp^3 bonded carbon. Crystallization in the amorphous layer also includes chemical reactions, such as hydrogen abstraction, dehydrogenation of absorbed complexes, recombination of hydrogen atoms, etc. During the crystallization, carbon atoms rearrange towards {111} planes to achieve the minimum surface energy. The crystallized regions then act as nuclei for the subsequent growth of diamond. In steps IV to VI, diamond growth takes place. Carbon atoms added to the surface (step IV) diffuse inwards by a solid-state diffusion process. The initial diamond shape is hemispherical (step IV), as confirmed by examining a planar view of diamond growth on iron silicide by the same author. Once a diamond microcrystal reaches a critical size (step V), it will acquire a faceted crystallographic shape characterized by defects such as points, stacking faults and twins (step VI). In step VII, secondary nucleation takes place as a result of the concentration fluctuation on the surface of the diamond crystal. This fluctuation leads to an uneven surface of the disordered domain; its thickness varies from 8 to 14 nm, depending on deposition conditions. Once the thickness of the disordered domain exceeds the critical thickness (>15 nm), there will not be enough localized thermal energy or time available for carbon atoms to diffuse into the diamond crystal, leading to the secondary nucleation on the surface.

The formation of the DLC interlayer has also been observed by other investigators in the experiments examining diamond nucleation on Mo substrates [21,37] and Si substrates [10,11,30,35,61]. It was found that diamond crystallites are not located directly on the substrates but on an intermediate amorphous layer. Nucleation of diamond occurs readily on the disordered carbon surfaces, and the formation of this type of intermediate layers is indeed one step in the diamond nucleation mechanism.

Nucleation on an intermediate layer of metal carbide

Badzian and Badzian [64] suggested that diamond nucleation on Si is preceded by the formation of a β-SiC buffer layer, and nucleation occurs on the surface of the carbide. This is supported by many growth experiments of diamond particles or films on Si substrates in HFCVD and MW PACVD [12,14,23,28,29,40,62,65-67], which showed that the Si surface is indeed transformed to SiC under conditions leading to diamond growth, and diamond nucleation occurs on the SiC intermediate layer. A recent AFM study [25] provided further evidence for the formation of SiC. The formation of a Mo carbide layer in the initial stage of diamond film deposition was reported in DC arc discharge CVD [63] and MW PACVD [16,69]. In diamond growth experiments on Mo and Si substrates using MW PACVD by Meilunas et al. [69], Mo_2C and SiC layers of approximately 1.5 μm and 10 nm in thickness were observed with SEM within 1 min and after 5 min, respectively. The growth rate of SiC was much less than that of Mo_2C. Diamond nanocrystallites were observed after 1 min, and no further carbide layer growth was detected once the surface was covered with diamond.

Joffreau et al. [68] and Lindlbauer [73] conducted systematic studies of diamond growth on carbide-forming refractory metals and observed that diamond nucleation occurred only after the formation of a thin carbide layer. Lux and Haubner [72] subsequently postulated a model to elucidate the mechanism governing the nucleation process on a carbide-forming substrate (Figure 2). It was suggested that carbon dissolves into the substrate initially, resulting in the formation of a stable carbide. Diamond nucleation occurs on the carbide layer when the carbon concentration on the surface reaches its saturation value. Lux and Haubner [72] also compared the time evolution of nucleation densities on Ti, Hf, Nb, Ta, Mo, and W, and found that the difference in the nucleation densities is related to the solubility and/or diffusivity of carbon in the respective substrates. The incubation period for nucleation is the shortest on the metal that can most rapidly achieve a supersaturation of carbon on the surface.

Nucleation on an intermediate layer of graphite

Microbalance studies of diamond nucleation on Pt [71] showed an initial incubation period during which an oriented graphite deposit formed. The deposit subsequently disappeared, and the final deposit contained only polycrystalline diamond. Several other experiments on Ni and Pt in

HFCVD [17], on Si [19] and Cu [32,34,62] in MW PACVD have also provided direct evidence for the formation of graphite on the substrates prior to diamond nucleation. It was found that the graphite film formed initially on the substrate surface greatly enhanced diamond nucleation [32,34].

On the basis of these experimental findings and variable metric static energy minimization calculations, Lambrecht et al. [13] proposed a detailed nucleation mechanism, as shown schematically in Figure 3. It was suggested that graphite initially condenses on the substrate surface and the $\{1\bar{1}00\}$ prism planes are subsequently hydrogenated. Diamond nuclei grow preferentially on the prism planes of graphite, with kinetically preferential nucleation at the emerging graphite stacking faults, and with an almost perfect interface between graphite and the diamond nuclei. There exists a preferential epitaxial lattice registry relationship between graphite and diamond, i.e., $(111)_{\text{diamond}} \parallel (0001)_{\text{graphite}}$ and $(110)_{\text{diamond}} \parallel (1120)_{\text{graphite}}$ [32,34,71]. This relationship means that the puckered six-member rings in the diamond (111) plane retain the same orientation as the flat six-member rings in the graphite (0001) basal plane. Etching of graphite occurs simultaneously during diamond nucleation. Atomic hydrogen, known to be important in diamond growth, also plays an important role in nucleation: by terminating the dangling surface bonds it stabilizes sp^3 nuclei with respect to sp^2 nuclei. It also serves as a reactive solvent which permits the conversion of graphite nuclei into diamond nuclei, hence circumventing the large activation barrier between graphite and diamond. Lambrecht et al. [13] stated that this detailed nucleation mechanism is the dominant channel for the spontaneous nucleation of new independent diamond crystals in the absence of pre-existing diamond seeds. They indicated that the elimination of graphite precursors is necessary for the suppression of secondary nucleation, which limits the growth of large diamond single crystals. On the other hand, for faster growing highly oriented, epitaxial, polycrystalline diamond films, enhancing nucleation with graphite precursors is desirable during the early stages of heteroepitaxial deposition, when rapid coalescence of oriented diamond nuclei is required. The epitaxial relationship of diamond with graphite may provide important clues for new routes to heteroepitaxy if methods can be found to orient the initial graphitic precursors.

It should be noted, however, what intermediate layers form depends not only on substrate materials and pretreatment methods but also on deposition conditions. For example, Belton and Schmieg [17] have observed distinctly different intermediate layers on different substrates in HFCVD of diamond. Their experiments showed that graphite carbon deposited on Pt substrates, while a thick graphite layer developed on Ni substrates prior to diamond nucleation. Diamond eventually nucleated on defect sites in these graphite deposits. Moreover, different gas compositions can produce different intermediate layers on the same substrate. In MW PACVD of diamond on a Si substrate scratched with diamond paste, Williams et al. [65,67] found that an interfacial single-crystal β-SiC layer grew for 0.3% CH_4 in H_2, whereas an amorphous layer,

instead of the SiC layer, was observed for 2% CH_4 in H_2. Hence, it is safe to say that the formation of the interlayers is a step in the spontaneous nucleation process of diamond on non-diamond substrates, but this alone is not sufficient for nucleation to occur [40]. Surface carbon saturation and defects or high-energy sites [33,60], present in a-C:H or a-C intermediate layers [21,37], in carbide layers (due to island growth of carbides and carbon accumulation on carbides [40]), or in graphite layers [17], constitute a sufficient condition for diamond nucleation on these interlayers.

Surface nucleation process can be described with two quantities: surface nucleation density, N_d (cm^{-2}), and surface nucleation rate, N_r (cm^{-2} h^{-1}). The nucleation density is the number of nuclei grown on unit substrate surface, and the nucleation rate is the number of nuclei formed per unit substrate surface in unit time. The nucleation density depends on the number of activated nucleation sites available on the substrate surface. Nucleation will stop when crystals have nucleated on all available nucleation sites or when the diffusion zones of nuclei overlap each other. Surface nucleation densities and rates on non-diamond substrates vary from 10^3 to 10^{11} cm^{-2} [24,39,40,41,74-78], and from 10^3 to 10^8 cm^{-2} h^{-1} [79] (10^9 to 10^{10} cm^{-2} h^{-1}, as estimated from the measured data in [40]), respectively, depending on substrate materials, surface pretreatment methods, and synthesis conditions.

2.3. Substrate materials

Substrate materials may be classified into three major groups in terms of carbon/substrate interactions [72], as listed in Table 2.

Table 2. Classification of substrate materials [72]

Little or no solubility or reaction		Diamond, graphite, carbons, Cu, Ag, Au, Sn, Pb, etc.
C-diffusion only,C dissolves in MeC mixed crystals		Pt, Pd, Rh, etc.
Carbide formation		
	metallic	Ti, Zr, Hf, V, Nb, Ta, Cr, Mo, W, Fe, Co, Ni(metastable)
	covalent	B, Si, etc.
	ionic	Al, Y, rare earth metals, etc.

The physical parameters of currently used and potential substrate materials are summarized in Tables 3 and 4. Diamond surfaces or particles provide the best nucleation potential [72,79,88-90]. Nucleation on cBN readily occurs [91-94]. Nucleation rates on stable carbide-forming substrates (Si, Mo, W) are one to two orders of magnitude higher than on non-carbide-forming substrates (Cu, Au) [79]. Among carbide-forming substrates (Si, Mo, Al, Ni, Ti), the nucleation density on Mo is about one order of magnitude higher than on all other substrates under the same deposition conditions [95]. Nucleation rates are several times higher on polycrystalline substrates than on single-crystal substrates of the same material after identical surface pretreatment [46,79].

Refractory metal carbides (TaC, WC, Mo_2C) and some covalent carbides (SiC, B_4C) have a positive effect on nucleation, while effects of ionic carbides (Al_4C_3, liquid salts, etc.) on nucleation are less known [72]. Nucleation occurs readily on substrates forming amorphous DLC (mostly Mo and Si) without any pretreatment [21,35,37]. Graphite interlayers or particles form mostly on Ni, Pt, Cu, and Si [17,19,32,34,62,71], and favor diamond nucleation [13,32,34,71].

Table 3. Physical parameters of currently used or potential substrate materials for diamond epitaxy

Substrate material	Melting point[a] (°C)	Lattice constant[b] (Å)	Density[c] (kg m^{-3})	C diffusivity[d] (cm^2 s^{-1})	Thermal expansion coefficient[e] (10^{-6} K^{-1})	Surface energy[f] (J m^{-2})
diamond (cubic)	3057 [80]	3.567 [2]	3515 [2]	----	0.8 [2]	5.3 (111) [2]
(hexagonal)	----	----	3520 [2]	----	----	6.5 (110) [2]
a-axis	----	2.52 [2]	----	----	----	9.2 (100) [2]
c-axis	----	1.42 [2]	----	----	----	
graphite (hexagonal)	3797 [80]	----	2260 [2]	----	----	
a-axis	----	2.46 [2]	----	----	negative [2]	2.80 (10 $\bar{1}$0) [81]
c-axis	----	6.71 [2]	----	----	25 [2]	0.17 (0001) [82]
cBN (cubic)	2727 [83]	3.615 [83]	3490 [83]	----	0.59 [83]	
Si (diamond-cubic)	1412 [84]	5.42 [84]	2340 [84]	$7\cdot10^{-15}$ [83]	7.6 [84]	1.46 (111) [2]
Cu (fcc)	1084 [84]	3.61 [84]	8960 [84]	----	17.0 [84]	2.08 (100) [32]
Fe (γ) 912-1400°C(fcc)	1536 [84]	3.56 [84]	7400 [84]	$2\cdot10^{-7}$ [83]	>14.6 [84]	
Fe (α) <912°C (bcc)	----	2.86 [84]	7870 [84]	$8\cdot10^{-7}$ [83]	12.1 [84]	2.939/1.923 [85]
Ni (fcc)	1455 [84]	3.52 [84]	8900 [84]	$2\cdot10^{-8}$ [84]	13.3 [84]	2.364/1.773 [85]
Co (α) (hcp)	----	2.51,4.07 [84]	8900 [84]	----	12.5 [84]	
(β) >390 °C (fcc)	1494 [84]	3.54 [84]	----	$1\cdot10^{-8}$ [84]	----	2.709/2.003 [85]
β-SiC (cubic)	2697 [83]	4.35 [84]	3210 [83]	----	4.63 [83]	
Y-ZrO_2 (cubic)	2850 [83]	5.07 [86]	5560 [83]	----	4.0 [83]	

[a] at 1 atm.

[b] at room temperature, or at the temperatures at which the phases exist.

[c] at 20 °C.

[d] calculated at 800 °C for most metals; or at the lower limit of temperature range for the phases existing above 800 °C.

[e] 0-100 °C for metals, diamond and graphite; 25-500 °C for ceramics.

[f] surface energy at 25 °C / surface energy at melting temperature. The surface energies do not include the effects of surface reconstruction, physisorption/chemisorption, or other surface reactions.

2.4. Surface pretreatment methods and nucleation enhancement mechanisms

Surface pretreatment methods include scratching, seeding, electrical biasing, covering/coating, ion implantation, pulsed laser irradiation, and carburization. Diamond nucleation on non-diamond surfaces can be enhanced by the surface pretreatments, with ultrasonic-scratching and biasing having the best efficacy on nucleation enhancement, followed by scratching, seeding, covering/coating, and ion implantation, etc., as summarized in Table 5. Nucleation on pretreated surfaces is observed to occur primarily on carbon-rich particles or defects, such as scratches,

grain boundaries, particle boundaries, dislocations, electron bombardment damages, and edges of etch pits/craters [39,72,75,79].

Table 4. Physical parameters of currently used and potential substrate materials and their carbides, nitrides, or oxides

Substrate material	Melting point[a] (°C)	Lattice constant[b] (Å)	Density[c] (kg m^{-3})	C diffusivity[d] (cm^2 s^{-1})	Thermal expansion coefficient[e] (10^{-6} K^{-1})	Surface energy[f] (J m^{-2})
Al (fcc)	660 [84]	4.04 [84]	2700 [84]		23.5 [84]	1.085/0.939 [85]
Al_4C_3 (rhombic)	2200 [87]	3.33,24.94 [84]	2950 [87]	----		
AlN (hexagonal)	2202 [83]	3.10,4.97 [84]	3300 [83]	----	4.84 [83]	
Au (fcc)	1064 [84]	4.07 [84]	19300 [84]	----	14.1 [84]	1.626/1.345 [85]
Pt (fcc)	1770 [84]	3.92 [84]	21450 [84]		9.0 [84]	2.691/2.055 [85]
Fe_3C (orthorhombic)	1650 [87]	4.52,5.09,6.75 [84]	7400 [87]	----	6.0 [87]	
Ti (α) <900°C (hcp)	----	2.95,4.68 [84]	4500 [84]	$7\cdot10^{-9}$ [84]	8.9 [84]	
(β) >900°C (bcc)	1667 [84]	3.29 [84]	4110 [84]	$2\cdot10^{-6}$ [83]	9.9 [84]	2.570/1.723 [85]
TiN (cubic)	2927 [83]	4.24 [84]	5430 [83]	----	9.35 [83]	
TiC (fcc)	3160 [83]	4.32 [84]	4920 [83]	----	6.52 [83]	
Nb (bcc)	2467 [84]	3.294 [84]	8600 [84]	$3\cdot10^{-12}$[83]	7.2 [84]	2.983/2.022 [85]
NbC (bcc)	3497 [83]	4.424-4.457 [84]	7820 [87]	----	6.52 [87]	
Ta (bcc)	2980 [84]	3.30 [84]	16600 [84]	10^{-14} [72]	6.5 [84]	3.018/2.270 [85]
TaC (fcc)	3540 [83]	4.45 [84]	14480 [83]	----	6.29 [83]	
Cr (α) <1840°C (bcc)	1860 [84]	2.89 [84]	7100 [84]	$4\cdot10^{-8}$ [83]	6.5 [84]	2.056/1.913 [85]
Cr_3C_2 (orthorhombic)	1895 [83]	2.82,5.52,11.46[84]	6700 [83]	----	8.00 [83]	
Mo (bcc)	2615 [84]	3.14 [84]	10200 [84]	10^{-11} [84]	5.1 [84]	2.877/2.116 [85]
Mo_2C (hcp)	2690 [83]	3.01,4.74 [84]	9180 [87]	----	7.8–9.3 [5]	
W (α) (bcc)	3387 [84]	3.16 [84]	19300 [84]	10^{-13} [83]	4.5 [84]	3.468/2.487 [85]
WC (hcp)	2627 [87]	2.90,2.83 [84]	15800 [83]	----	4.42 [83]	
W_2C (hcp)	2776 [80]	2.99,4.71 [84]	17150 [87]	----	3.58 [87]	
Zr (α)<840°C (hcp)	----	3.23,5.14 [84]	6490 [84]	$8\cdot10^{-11}$[84]	5.9 [84]	
(β)>840°C (bcc)	1852 [84]	3.61 [84]	5800 [84]	$3\cdot10^{-8}$ [84]	----	2.790/1.554 [85]
ZrC (fcc)	3260 [83]	4.67 [84]	6660 [83]	----	6.1 [83]	
Hf (α)<1310°C (hcp)	----	3.19,5.20 [84]	13100 [84]	10^{-13} [72]	6.0 [84]	
(β) >1310°C (bcc)	2227 [84]	3.50 [84]	----	----	----	3.333/1.701 [85]
HfC (fcc)	3887 [87]	4.46 [84]	12520 [83]	----	6.27 [83]	
V (bcc)	1902 [84]	3.024 [84]	6100 [84]	$1\cdot10^{-8}$ [84]	8.3 [84]	2.876/2.082 [85]
VC (fcc)	3327 [83]	4.17 [84]	5770 [87]	----	7.2 [87]	
Si_3N_4 (β)(hexagonal)	2442 [83]	7.603,2.909 [84]	3187 [83]	----	2.11 [83]	
SiO_2 (hexagonal)	1710 [84]	3.464,4.382 [86]	2320 [84]	----	0.55 [84]	
B_4C (rhombohedral)	2447 [83]	5.60,12.12 [84]	2510 [83]	----	4.5 [83]	
Al_2O_3 (hexagonal)	2049 [83]	4.785,12.991 [83]	3970 [83]	----	7.5 [83]	

[a] at 1 atm.

[b] at room temperature, or at the temperatures at which the phases exist.

[c] at 20 °C.

[d] calculated at 800 °C for most metals; or at the lower limit of temperature range for the phases existing above 800 °C.

[e] 0-100 °C for metals, diamond and graphite; 25-500 °C for ceramics.

[f] surface energy at 25 °C / surface energy at melting temperature. The surface energies do not include the effects of surface reconstruction, physisorption/chemisorption, or other surface reactions.

Table 5. Typical surface nucleation densities of diamond after various surface pretreatments

Pretreatment method	Nucleation density (cm^{-2})	Reference
No pretreatment	$10^3 - 10^5$	[41,75,76]
Scratching	$10^6 - 10^{10}$	[39-41,77,96]
Ultrasonic scratching	$10^7 - 10^{11}$	[39,75,78]
Seeding	$10^6 - 10^{10}$	[97,98]
Biasing	$10^8 - 10^{11}$	[40,99]
Covering/Coating with		
Fe film	4.84×10^5	[100]
graphite film	10^6	[101]
graphite fiber	$>10^9$	[102]
a-C film	3×10^{10}	[30]
C_{70} clusters + biasing	= seeding effect	[26]
Y-ZrO_2 , a-BN, SiC layer	enhancement	[14,18,103,104]
C^+ ion implantation on Cu	enhancement	[32]
As^+ ion implantation on Si	$10^5 - 10^6$	[105]
Pulsed laser irradiation + coating a-C, WC, cBN layer	enhancement	[106]
Carburization	enhancement	[31,70]

As schematically depicted in Figure 4 [72], nucleation enhancement by scratching is attributed to (a) seeding effect [78,98,107], (b) minimization of interfacial energy on sharp convex surfaces [20,108], (c) breaking of a number of surface bonds or presence of a number of dangling bonds at sharp edges [100], (d) strain field effects [105], (e) rapid carbon saturation (fast carbide formation) at sharp edges [72,109], and (f) removal of surface oxides [39,100]. Another possible operating mechanism [13,71] for the nucleation enhancement by scratching is that scratching produces non-volatile graphitic particles through local pyrolysis of absorbed hydrocarbons. These graphitic clusters would be subsequently hydrogenated in the atomic hydrogen environment under the typical CVD conditions to form the precursor molecules. The efficacy of scratching on different substrates descends in the order from Si, Mo, to WC substrates [24]. Abrasives used for scratching pretreatment include diamond, oxides, silicides, nitrides, carbides and borides. The effect of the abrasives on nucleation enhancement increases in the following order: silicides < SiO_2 < nitrides < ZrO_2 < carbides < borides < Al_2O_3 < cBN < diamond [110,111]. As shown in Figure 5 [39], nucleation density decreases with increasing particle size of diamond abrasive paste in the polishing pretreatment (Figure 5(a)), but increases with increasing particle size in the

ultrasonic scratching pretreatment (Figure 5(b)). Generally, however, the optimal size of abrasive particles depends on pretreatment methods, deposition processes, growth conditions, and nature of substrate materials [72,77,111-116]. The size and physical properties of the abrasives used for scratching pretreatment are summarized in Table 6.

Table 6. Size and physical properties of diamond and various ceramic compounds used for scratching pretreatment

Abrasive material	Particle size (μm)	Density ($kg\ m^{-3}$)	Hardness ($kg\ mm^{-2}$)	Crystal structure
Diamond	0.25–40 (ultrasonic) [39,113] 0.25–15 [39,77,114]	3515 [2]	5700–10400 [2]	Cubic/hexagonal [2]
Oxides				
Al_2O_3	0.3–1 [41,72,115]	3970 [83]	2000 [83]	Hexagonal [83]
ZrO_2	0.1–0.3 [111]	5560 [83]	1019 [83]	Cubic [83]
SiO_2	[111]	2320 [84]	790 [83]	Hexagonal [86]
Borides [110]				
TiB_2	2–10	4530	3370	Hexagonal
CrB	5–20	6110	1250	Orthorhombic
ZrB_2	5–15	6090	2252	Hexagonal
NbB_2	0.5–1	7000	2600	Hexagonal
MoB	1–5	8670	2350	Tetragonal
LaB_6	10–40	4720	2770	Cubic
TaB_2	0.5–1	12620	2500	Hexagonal
WB	1–5	15730	3700	Tetragonal
Carbides [110]				
B_4C	10–20	2510	2750	Rhombohedral
SiC	5–20	3220	2550	Hexagonal
TiC	10–30	4920	3170	Cubic
V_8C_7	20–40	5480	2480	Cubic
Cr_3C_2	2–10	6740	1800	Orthorhombic
ZrC	2–10	6660	2950	Cubic
NbC	10–30	7820	2170	Cubic
Mo_2C	0.5–3	9180	1499	Hexagonal
TaC	10–20	14400	1720	Cubic
WC	20–30	15770	1716	Hexagonal
Nitrides [110]				
BN	8–12	3480	4530	Cubic
AlN	1–10	3260	1200	Hexagonal
Si_3N_4	0.2–1	3180	2100	Hexagonal
TiN	3–15	5440	2050	Cubic
VN	1–5	6100	1310	Cubic
Cr_2N	0.5–3	6510	1571	Hexagonal
ZrN	3–15	7350	1670	Cubic
NbN	5–30	8310	1461	Cubic
TaN	1–5	14360	2416	Hexagonal

Silicides [110]				
$TiSi_2$	10–30	4040	892	Orthorhombic
$CrSi_2$	10–50	4980	1131	Hexagonal
$ZrSi_2$	10–30	4860	1063	Orthorhombic
$NbSi_2$	10–40	5660	1050	Hexagonal
$MoSi_2$	10–40	6240	1200	Tetragonal
$TaSi_2$	10–60	9100	1407	Hexagonal
WSi_2	5–15	9860	1074	Tetragonal

Dipping, spinning, spraying, and electrophoretic seeding have been employed to seed diamond, Si, Al_2O_3, or SiC on various substrates [117-120]. The residual diamond seed particles on the substrate surface are the predominant nucleation sites (or the seed particles themselves are nuclei) and diamond growth then occurs by means of homoepitaxy on these seed particles [98]. Nucleation density is linearly proportional to the diamond seed particle density (Figure 6 [98]), being approximately a tenth of the seed particle density [98]. Seeding also provides the possibility for epitaxial or highly oriented growth of diamond films on non-diamond substrates [38,121].

Biasing a substrate can help to reduce and suppress oxide formation on the substrate surface, remove native oxides [40], and overcome the energy barrier for the formation of stable diamond nuclei by more effectively activating the substrate surface and/or increasing the flux and mobility of adatoms [40,122], as schematically shown in Figure 7 [122]. In DC PACVD and HFCVD, positive substrate biasing is effective for increasing nucleation of diamond [123,124], while in MW PACVD both positive and negative biasing can enhance diamond nucleation [122]. By varying the duration of biasing pretreatment [40] and/or the applied voltage [122] and current [6], nucleation density can be controlled over three to six orders of magnitude (Figure 8 [122]). As evident from Figure 8, larger absolute values of substrate bias voltage lead to higher nucleation densities. At the same absolute values of substrate bias voltage and for CH_4 concentrations from 10 to 40%, the nucleation densities on negatively biased substrates are one or two orders of magnitude higher than those on positively biased substrates [122]. However, the attraction of cations in negative biasing leads to roughening of Si surfaces, whereas positively biased Si substrates maintain smooth surfaces [122]. Therefore, positive biasing is a more suitable pretreatment condition for Si substrates. With increasing bias current, the grain size and non-diamond carbon incorporation in diamond films decrease with concomitant increase in Young's modulus and fracture strength, while large compressive stresses in films decrease and turn to tensile stresses [6].

Nucleation enhancement has also been achieved by covering substrate surfaces with graphite fibers/clusters [33,60,102], or films [70,101], and coating substrate surfaces with thin films of metals (Fe, Cu, Ti, Nb, Mo, Ni) [31,104], C_{60}, C_{70} [26,125], a-C [30], DLC [126], Y-ZrO_2 [103], a-BN and SiC [14,18,104], or hydrocarbon oil [127], etc. The efficacy of the overlaid materials on nucleation enhancement decreases in the order from C_{70}, a-C, DLC, graphite fiber, graphite film, Fe, Cu, Ti, Ni, Mo, to Nb [26,30,100-102,104]. The thickness of the overlayers

ranges typically from a few nanometers (2–8 nm for metal films [104], 10–20 nm for hydrocarbon oil [127], 100 nm for a C_{70} layer [26], 150 nm for a Y-ZrO_2 layer [103]) to a few micrometers (~1 μm for carbon film [101]). The nucleation enhancement is attributed to the physical and chemical effects associated with changes to the surface (the overlayers promote carbon saturation at the substrate surface, and provide high-energy sites or nucleation centers [26,30,70,101,126]), and changes to the gas chemistry in the immediate vicinity of the substrate surface [101].

The ion implantation method has been used to modify the surface energy and surface structure of substrates in order to enhance diamond nucleation. Implantation of C^+ (10^{18} ions cm^{-2}, 65–120 keV) on Cu [32] and As^+ (10^{14} ions cm^{-2}, 100 keV) on Si [105,128] enhances diamond nucleation, while Ar^+ implantation (3×10^{15} ions cm^{-2}, 100 keV) on Si [129] decreases nucleation density. The lattice damages (strain, amorphous disorder and twinning) created by ion implantation are deemed to be responsible for nucleation enhancement [105]. The strain is probably the primary physical reason for diamond nucleation enhancement on ion implanted substrates [105].

Pulsed laser irradiation of a thin buffer layer of a-C, WC or cBN deposited on substrates (Cu, stainless steel, Si) leads to significant enhancement of both nucleation and adhesion of diamond films on the substrates [106]. It is speculated [106] that the irradiation converts a portion of the a-C on the surface into diamond or results in the formation of a reaction product that facilitates diamond nucleation. Carburization of substrates (Mo, W, Si, Fe/Si) also leads to nucleation enhancement due to the formation of carbides and the saturation of carbon at the substrate surface [29,31,70].

Scratching and seeding are simple and effective for diamond nucleation enhancement, but cause surface damage and contamination. These pretreatment methods cannot be easily applied to substrates of complex geometry and shape, and are incompatible with many applications requiring extremely smooth, clean surfaces, such as diamond films for electronic devices, optical window materials and smooth wear-resistant coatings. As an alternative, biasing or covering/coating substrate surfaces can yield high nucleation densities comparable to, or even over those achieved by seeding or scratching, without significantly damaging the surfaces, and therefore is of particular importance [101].

2.5. Deposition conditions

Deposition conditions, such as substrate temperature, gas pressure, gas composition, and gas activation, critically influence nucleation density and rate. It has been noted that ideal deposition conditions for growth may not be optimal for nucleation. For example, the *in vacuo* surface analyses and microstructure characterization of the diamond nucleation process on negatively biased Si substrates [40] revealed that the biasing could enhance nucleation significantly, whereas

a much poorer-quality diamond film was grown if the biasing was continued during the growth. Similarly, the optimal values of gas pressure and substrate temperature for growth are not identical to those for nucleation.

The optimal deposition conditions (ranges, values or tendency) for diamond nucleation reported in published literature are summarized in Table 7. An optimum substrate temperature exists near 860 ˚C (Figure 9 [96]), at which a maximum nucleation density can be achieved [42,47,96,116,130]. This overall dependence of nucleation density on substrate temperature is speculated [96] to be caused by the change in the adsorption state and surface diffusion length of growth precursors. The precursors are adsorbed on the substrate mainly by physical adsorption below 900 ˚C and predominantly by chemical adsorption above this temperature, resulting in an abrupt increase in the diffusion length of the precursors around 900 ˚C [96]. As a result, the capture rate of the precursors (sticking probability) on the substrate surface, and hence the nucleation rate and density, drastically increase when the substrate temperature approaches 860 ˚C.

Table 7. Optimum ranges and values of process parameters for diamond nucleation

Parameters	Optimum ranges, values or tendency
Substrate temperature	
MW PACVD	860 ˚C [96]
	830-860 ˚C [116]
HFCVD	900–1000 ˚C [47]
	850 ˚C [42,130]
Gas activation	
Filament temperature in HFCVD	2100 ˚C [43]
Discharge current in DC PACVD	N_d increases with increasing discharge current [45]
Power density	N_d increases with increasing power density [49]
Gas pressure	5 torr
MW PACVD	[16]
HFCVD	[12]
Gas composition	N_d increases with increasing CH_4 % in H_2
MW PACVD	[16,41,122,131,132]
HFCVD	[42,47]
Gas flow rate	N_d increases with increasing gas flow rate
hollow-cathode PACVD, HFCVD	[50]
Oxygen addition	
MW PACVD	Accelerates nucleation [44]
	Favors nucleation [16]
	2–10% O_2+ 2–15%CH_4 in H_2 [18]
HFCVD	Suppresses nucleation [17]
Arc plasma jet CVD	Decreases nucleation density, 33% O_2 [133]
Flame CVD	0.75–0.9 O_2/C_2H_2 [21]

The effect of filament temperature in HFCVD on nucleation is similar to that of substrate temperature, i.e., with increasing filament temperature, nucleation density initially increases, reaches a maximum at 2100 ˚C and decreases thereafter, with 2100 ˚C being a possible optimum

value [43]. The drop-off for T > 2100 ˚C is explained by the observation that the etching of nucleation sites is enhanced with increasing filament temperature [47].

In DC PACVD [45], a nucleation density of 6×10^9 cm^{-2} was achieved on untreated substrates by increasing the discharge current to 1 A and the cathode temperature to 1400 ˚C. It has also been suggested that nucleation can be enhanced by using high power density, such as in plasma jet, or DC plasma discharge CVD [49], in which H_2 and CH_4 dissociation is promoted.

Low gas pressures (~5 torr) [12,16], high CH_4 concentrations [16,41,42,47,122,131,132] (Figure 8), and/or high gas flow rates [50] lead to high nucleation densities. The pressure dependence of nucleation density is explained [12] by the competition effect between β-SiC formation, which increases the diamond nucleation density, and atomic-hydrogen etching, which decreases the number of nucleation sites. A high CH_4 concentration can promote carburization of the substrate surface and accelerate carbon saturation at the substrate surface [16], while a high gas flow rate may increase the mass transfer of gas species to the substrate surface. Consequently, diamond nucleation density can be enhanced.

The addition of oxygen in gas mixture can accelerate the saturation of carbon on the substrate surface, reduce the incubation period, and promote a much faster diamond nucleation and growth than with oxygen-less plasmas [44]. The presence of oxygen allows low substrate temperatures, preserves a good film quality at high CH_4 concentrations, and suppresses eventual surface contamination by Si [16]. However, the addition of oxygen is also reported to suppress diamond nucleation by etching nucleation sites (graphite) on Ni and Pt substrates [17]. An optimum oxygen concentration is found to be about 33% in arc plasma jet CVD [133], 2–10% in low pressure low temperature MW PACVD [18], and 0.75–0.9 O_2/C_2H_2 in flame CVD [21].

2.6. Modeling and theoretical studies

The current information about the size, structure and chemistry of diamond nuclei is primarily speculative, with a small number of conclusive results. It has been proposed that diamond nuclei are multiple twinned particles, likely containing some of the structures related to boat-boat conformer of bicyclodecane (10 carbon atoms) or boat-chair-chair-boat tetracyclooctadecane (18 carbon atoms) within higher molecular weight compounds formed by the partial hydrogenation of graphitic or polyaromatic hydrocarbons [134-137]. Such precursors are stable in the high temperature reducing atmosphere of CVD diamond growth. Indirect evidence for the presence of such molecular precursors has been found [138]. On the contrary, Frenklach and Wang [139], in a detailed chemical kinetics modeling of a HFCVD reactor, found that under the operating conditions typical for diamond deposition, atomic hydrogen suppresses the formation of the aromatics.

Compared to the significant development in nucleation enhancement methods, fundamental scientific issues related to the nucleation process remain less well addressed. In theoretical studies

on diamond nucleation, thermodynamic theory, homogeneous and heterogeneous chemical kinetics, classical nucleation theory, adsorption-desorption kinetics and equilibrium have been considered to predict preferential conditions for diamond nucleation and growth [74]. A narrow range of deposition conditions, such as pressure (supersaturation), temperature, and composition as well as state (structure, roughness, etc.) of the substrate surface, have been derived [74,82,140], under which nucleation and growth of diamond are significant and graphite is etched. The theoretical study [74] uncovered the crucial role of hydrogen atoms in stabilizing the diamond structure on the substrate surface relative to graphite. It was found that hydrogen may permit metastable growth of diamond by impeding the conversion of diamond to graphite at temperatures below 1300 ˚C [141]. The role of substrate surfaces in stabilizing the diamond structure has also been recognized [82].

However, most conditions in vapor deposition of thin films have been shown to be such that the critical nucleus size is on the order of a few atoms [142]. Under such conditions, the formation free energy of a critical nucleus may be negative [142] and the surface energy contribution may cause a reverse effect on the phase stability [140], a case referred to as nonclassical nucleation process [142]. In such a nucleation process, a nanometer-sized diamond nucleus may be more stable at normal pressure than a graphite nucleus containing the same number of atoms [140,143]. A quantitative calculation [143] revealed that surface energies are an important aspect in the stabilization of nanocrystalline diamonds, and for surface bonds terminated with hydrogen atoms, diamonds smaller than ~3 nm in diameter are energetically favored over polycyclic aromatics (the precursors to graphite). Therefore, in the nonclassical nucleation process, the surface energy contribution must be evaluated on the basis of a microscopic picture of a nucleus [142], and atomistic theory should be employed as the starting point of theoretical analyses.

Theoretical modeling studies on the kinetic aspect of diamond nucleation are scarce. In spite of the attempts made in [42,130,142,144], the approach employed requires an accurate estimation of the kinetic rate constants, which has been made by fitting the model to experimental data, and hence is system- (or experiment)-dependent. The kinetics of impingement and surface diffusion of adatoms, as well as the formation of intermediate carbonaceous phases have not been considered in these studies. In addition, the kinetic scheme used in these studies is unable to distinguish between a metal surface and its carbide surface. A complete kinetic model is, therefore, expected to contribute to a better understanding of the role of the intermediate carbonaceous phases in diamond nucleation and to be able to describe the entire time evolution of the nucleation, including the events occurring during the incubation period.

3. Conclusion

It is evident from published literature that technological problems associated with the nucleation of polycrystalline diamond films have been adequately addressed, as demonstrated by the development of the numerous methods for nucleation enhancement, selective nucleation, and textured/oriented growth. However, the scientific issues integral to the nucleation process remain less well understood. A clear picture of diamond nucleation in CVD is still needed to provide insight into the nucleation kinetics. A comprehensive theoretical model is required to achieve a thorough understanding of the nucleation process and to obtain more reproducible and predictable results.

Acknowledgment

This work has been supported by the Materials Science Program at ARPA (Contract N00014-93-1-2002).

References

1 National Materials Advisory Board, *Status and applications of diamond and diamond-like materials: an emerging technology*, NMAB-445, National Academy Press (1990).

2 H.O. Pierson, *Handbook of carbon, graphite, diamond and fullerenes*, Noyes Publications, Park Ridge, New Jersey, USA (1993); J.E. Field, *The properties of diamond*, Academic Press, London (1979).

3 S.B. Qadri, C. Kim, E.F. Skelton, T. Hahn and J.E. Butler, *Thin Solid Films*, **236** (1-2) (1993) 103.

4 Y. Seino and S. Nagai, *J. Mater. Sci. Lett.*, **12** (5) (1993) 324.

5 M.S. Wong, R. Meilunas, T.P. Ong and R.P.H. Chang, *Appl. Phys. Lett.*, **54** (20) (1989) 2006.

6 K. Baba and Y. Aikawa, *NEC Research and Development*, **34** (2) (1993) 176.

7 J.E. Graebner, S. Jin, G.W. Kammlott, B. Bacon and others, *J. Appl. Phys.*, **71** (11) (1992) 5353.

8 X. Jiang, K. Schiffmann, A. Westphal and C.-P. Klages, *Appl. Phys. Lett.*, **63** (9) (1993) 1203; X. Jiang, K. Schiffmann and C.P. Klages, *Phys. Rev. B*, **50** (12) (1994) 8402.

9 J. Singh, *J. Mater. Sci.*, **29** (10) (1994) 2761.

10 R. Csencsits, J. Rankin, R.E. Boekenhauer, M.K. Kundmann and others, in *Evolution of Surface and Thin Film Microstructure Symposium*, ed. H.A. Atwater, E. Chason, M.H. Grabow and M.G. Lagally, Pittsburgh, USA (1993) 695.

11 K. Tamaki, Y. Watanabe, Y. Nakamura and S. Hirayama, *Thin Solid Films*, **236** (1-2) (1993) 115.

12 D. Kim, H. Lee, J. Lee, *J. Mater. Sci.*, **28** (24) (1993) 6704.

13 W.R.L. Lambrecht, C.H. Lee, B. Segall, J.C. Angus and others, *Nature*, **364** (6438) (1993) 607.

14 G.A. Hirata, L. Cota-Araiza, M. Avalos-Borja, M.H. Farfas and others, *J. Phys.: Condensed Matter*, **5** (33A) (1993) A305.

15 J. Singh and M. Vellaikal, *J. Appl. Phys.*, **73** (6) (1993) 2831.

16 P. Bou, L. Vandenbulcke, R. Herbin and F. Hillion, *J. Mater. Res.*, **7** (8) (1992) 2151.

17 D.N. Belton and S.J. Schmieg, *Thin Solid Films*, **212** (1-2) (1992) 68.

18 Y.H. Shing, F.S. Pool and D.H. Rich, *Thin Solid Films*, **212** (1-2) (1992) 150.

19 M.M. Waite and S.I. Shah, *Appl. Phys. Lett.*, **60** (19) (1992) 2344.

20 P.A. Dennig and D.A. Stevenson, *Appl. Phys. Lett.*, **59** (13) (1991) 1562.

21 K.V. Ravi, C.A. Koch, H.S. Hu and A. Joshi, *J. Mater. Res.*, **5** (11) (1990) 2356.

22 P.E. Pehrsson, F.G. Celii and J.E. Butler, in *Diamond Films and Coatings, Development, Properties, and Applications*, R.F. Davis, Noyes Publications, Park Ridge, New Jersey, (1993) 68.

23 D.N. Belton, S.J. Harris, S.J. Schmieg, A.M. Weiner and others, *Appl. Phys. Lett.*, **54** (5) (1989) 416.

24 W.A. Yarbrough and R. Messier, *Science*, **247** (4943) (1990) 688.

25 M.A. George, A. Burger, W.E. Collins, J.L. Davidson, A.V. Barnes and N.H. Tolk, *J. Appl. Phys.*, **76**(7) (1994) 4099.

26 R.J. Meilunas and R.P.H. Chang, *J. Mater. Res.*, **9** (1) (1994) 61.

27 Z. Feng, K. Komvopoulos, I.G. Brown and D.B. Bogy, *J. Mater. Res.*, **9** (8) (1994) 2148.

28 B.R. Stoner, S.R. Sahaida, J.P. Bade, P. Southworth and others, *J. Mater. Res.*, **8** (6) (1993) 1334.

29 S.D. Wolter, B.R. Stoner, J.T. Glass, P.J. Ellis and others, *Appl. Phys. Lett.*, **62** (11) (1993) 1215.

30 P.N. Barnes and R.L.C. Wu, *Appl. Phys. Lett.*, **62** (1) (1993) 37.

31 K. Kobayashi, T. Nakano, N. Mutsukura and Y. Machi,*Vacuum*, **44** (1) (1993) 1.

32 T.P. Ong, F. Xiong, R.P.H. Chang and C.W. White, *J. Mater. Res.*, **7** (9) (1992) 2429.

33 P.E. Pehrsson, J. Glesener and A. Morrish, *Thin Solid Films*, **212** (1-2) (1992) 81.

34 T.P. Ong, F. Xiong, R.P.H. Chang and C.W. White, *Appl. Phys. Lett.*, **60** (17) (1992) 2083.

35 J.J. Dubray, C.G. Pantano, M. Meloncelli and E. Bertran, *J. Vacuum Sci. & Technol. A*, **9** (6) (1991) 3012.

36 J.S. Ma, H. Kawarada and A. Hiraki, *Solid State Phys.*, **26** (8) (1991) 496.

37 K.V. Ravi and C.A. Koch, *Appl. Phys. Lett.*, **57** (4) (1990) 348; K.V. Ravi, *J. Mater. Res.*, **7** (2) (1992) 384.

38 P.C. Yang, W. Zhu and J.T. Glass, *J. Mater. Res.*, **8** (8) (1993) 1773.

39 P. Ascarelli and S. Fontana, *Appl. Surf. Sci.*, **64** (4) (1993) 307.

40 B.R. Stoner, G.-H.M. Ma, S.D. Wolter and J.T. Glass, *Phys. Rev. B* , **45** (19) (1992) 11067.

41 R.A. Bauer, N.M. Sbrockey and W.E. Brower, Jr., *J. Mater. Res.*, **8** (11) (1993) 2858.

42 E. Molinari, R. Polini, V. Sessa, M.L. Terranova and others, *J. Mater. Res.*, **8** (4) (1993) 785.

43 S. Park and J. Lee, *J. Mater. Sci.*, **28** (7) (1993) 1799.

44 S.I. Shah and M.M. Waite, *Appl. Phys. Lett.*, **61** (26) (1992) 3113.

45 Y. Hibino and Y. Hayashi, *Surf. Coat. Technol.*, **54-55** (1-3) (1992) 365.

46 B.V. Derjaguin and D.V. Fedoseev, *Scientific American*, **233** (5) (1975) 102.

47 J.W. Kim, Y.J. Baik and K.Y. Eun, in *Applications of Diamond Films and Related Materials*, ed. Y. Tzeng, M. Yoshikawa, M. Murakawa and A. Feldman, Elsevier Sci. Publ., (1991) 399.

48 J. Singh, M. Vellaikal and R. Dat, *Thin Solid Films*, **238** (1) (1994) 133.

49 L. Vandenbulcke, P. Bou and G. Moreau, *J. Electrochem. Soc.*, **138** (10) (1991) 2985.

50 B. Singh, O.R. Mesker, A.W. Levine and Y. Arie, *Proc. SPIE*, **877** (1988) 70.

51 C. Wild, N. Herres and P. Koidl, *J. Appl. Phys.*, **68** (3) (1990) 973; R. Kohl, C. Wild, N. Herres, P. Koidl and others, *Appl. Phys. Lett.*, **63** (13) (1993) 1792; R. Locher, C. Wild, N. Herres, D. Behr and P. Koidl, *Appl. Phys. Lett.*, **65** (1) (1994) 34; C. Wild, R. Kohl, N. Herres, W. Mueller-Sebert and P. Koidl, *Diamond and Related Materials*, **3** (1994) 373.

52 S. Mitura, *J. Cryst. Growth*, **80** (1987) 417.

53 M. Frenklach, R. Kematick, D. Huang, W. Howard and others, *J. Appl. Phys.*, **66** (1) (1989) 395; W. Howard, D. Huang, J. Yuan, M. Frenklach and others, *J. Appl. Phys.*, **68** (3) (1990) 1247; M. Frenklach, W. Howard, D. Huang, J. Yuan and others, *Appl. Phys. Lett.*, **59** (5) (1991) 546.

54 P.R. Buerki and S. Leutwyler, *J. Appl. Phys.*, **69** (6) (1991) 3739.

55 S. Matsumoto and Y. Matsui, *J. Mater. Sci.*, **18** (1983) 1785.

56 S.A. Godleski, P.V. Schleyer, E. Osawa and W.T. Wipke, *Prog. Phys. Org. Chem.*, **13** (1981) 63; S.E. Stein, *Nature*, **346** (1990) 517.

57 Z. Ajji, M. Buck, H. Schwenk and Ch. Wöll, Presentation in *41st National Symposium and 3rd International Conference on Nanometer-Scale Science & Technology*, American Vacuum Society, Denver, Colorado, Oct. 24-28, (1994) 137.

58 F.C. Frank and J.H. van der Merwe, *Proc. Royal Soc. London Ser. A*, **198** (1949) 205; M. Volmer and A. Weber, *Z. Phys. Chem.*, **119** (1926) 277.

59 M. Yoshikawa, *Diamond Films and Technol.*, **1** (1991) 1.

60 P.E. Pehrsson, J. Glesener and A.A. Morrish, in *Wide Band Gap Semiconductors Symposium*, Boston, MA, USA, 2-6 Dec. 1991, ed. T.D. Moustakas, J.I. Pankove and Y. Hamakawa, Pittsburgh, PA, USA, MRS (1992) 57.

61 C. Trevor, D. Cherns and P. Southworth, in *Proc. Institute of Phys. Electron Microscopy and Analysis Group Conf.*, Bristol, UK, 10-13 Sept. 1991, ed. F.J. Humphreys, Bristol, UK, IOP (1991) 275.

62 S.D. Wolter, B.R. Stoner, G.-H.M. Ma and J.T. Glass, in *Novel Forms of Carbon Symposium*, ed. C.L. Renschler, J.J. Pouch and D.M. Cox, Pittsburgh, USA, MRS (1992) 347.

63 A.A. Smolin, S.M. Pimenov, V.G. Ralchenko, T.V. Kononenko and others, *Diamond Films and Technol.*, **3** (1) (1993) 1.

64 A.R. Badzian and T. Badzian, *Surf. Coat. Technol.*, **36** (1988) 283.

65 B.E. Williams and J.T. Glass, *J. Mater. Res.*, **4** (1989) 373.

66 S. Yugo, T. Kimura and T. Muto, *Vacuum*, **41** (1990) 1364.

67 B.E. Williams, J.T. Glass, R.F. Davis and K. Kobashi, *J. Crystal Growth*, **99** (1990) 1168.

68 P.O. Joffreau, R. Haubner and B. Lux, *Int. J. Ref. Hard Mater.*, **7** (4) (1988) 186.

69 R. Meilunas, M.S. Wong, K.C. Sheng, R.P.H. Chang and R.P. VanDuyne, *Appl. Phys. Lett.*, **54** (22) (1989) 2204.

70 D. Michau, B. Tanguy, G. Demazeau, M. Couzi and others, *Diamond and Related Mater.*, **2** (1) (1993) 19.

71 J.C. Angus, A. Argoitia, R. Gat, Z. Li, M. Sunkara, L. Wang and Y. Wang, *Philosophical Transactions of the Royal Society, Series A,* **342** (1664) (1993) 195; Z. Li, L. Wang, T. Suzuki, A. Argoitia, P. Pirouz and J. Angus, *J. Appl. Phys.,* **73** (1993) 711.

72 B. Lux and R. Haubner, in *Diamond and Diamond-like Films and Coatings*, ed. R.E. Clausing, L.L. Horton, J.C. Angus and P. Koidl, Plenum Press, New York (1991) 579.

73 A. Lindlbauer, Ph.D. Thesis, TU-Vienna (1991).

74 B.V. Derjaguin and D.V. Fedoseev, *Surf. Coat. Technol.,* **38** (1989) 131.

75 G. Popovici and M.A. Prelas, *Physica Status Solidi A*, **132** (2) (1992) 233.

76 T. Hartnett, R. Miller, D. Montanari, C. Willingham and R. Tustison, *J. Vac. Sci. Technol. A,* **8** (1990) 2129.

77 Y. Cheng, C. Sho and G. Shu, *J. Cryst. Growth,* **99** (1990) 1196.

78 S. Iijima, Y. Aikawa and K. Baba, *J. Mater. Res.,* **6** (7) (1991) 1491.

79 B.V. Spitzyn, L.L. Bouilov and B.V. Derjaguin, *J. Crystal Growth,* **52** (1981) 219.

80 R. Hultgren, P.D. Desai, D.T. Hawkins, M. Gleiser and K.K. Kelley, *Selected values of the thermodynamic properties of binary alloys*, American Society for Metals, Metals Park, OH (1973).

81 R. Kern, in *Current Topics in Materials Science*, ed. E. Kaldis, North-Holland, Amsterdam, **12** (1985) 83.

82 E.S. Machlin, *J. Mater. Res.,* **3** (5) (1988) 958.

83 J. Shackelford and W. Alexander,*The CRC Materials Science and Engineering Handbook*, CRC Press,Boca Raton (1992).

84 E.A. Brandes, *Smithells Metals Reference Book*, 6th edition, Butterworth & Co, London (1983).

85 L.Z. Mezey and J. Giber, *Japn. J. Appl. Phys.,* **21** (11) (1982) 1569.

86 G.V. Samsonov, *The Oxide Handbook*, IFI/Plenum Data Corporation, New York (1973).

87 P.T.B. Shaffer, *Plenum Press Handbooks of High-Temperature Materials, No. 1 – Materials Index*, Plenum Press, New York (1964); G.V. Samsonov, *Plenum Press Handbooks of High-Temperature Materials, No. 2 – Properties Index*, Plenum Press, New York (1964).

88 E. Kondoh, K. Tanaka and T. Ohta, *J. Appl. Phys.,* **74** (3) (1993) 2030.

89 M. Komori, T. Maki, T. Kim, G. Hou and others, *Appl. Phys. Lett.,* **62** (6) (1993) 582.

90 Z.M. Zhang, H.M. Cheng, S.H. Li, Q.Y. Cai and others, *J. Cryst. Growth,* **132** (1-2) (1993) 200.

91 S. Koizumi, T. Murakami, T. Inuzuka and K. Suzuki, *Appl. Phys. Lett.,* **57** (6) (1990) 563.

92 W.A. Yarbrough, *J. Vacuum Sci. Technol. A,* **9** (1991) 1145.

93 W.P. Chai, Y.S. Gu, M. Li, Z.H. Mai and others, *J. Cryst. Growth,* **135** (3-4) (1994) 639.

94 R. Haubner, *J. Ref. Met.- Hard Mat.,* **9** (2) (1990) 70.

95 F. Akatsuka and F. Shimura, same as Ref. 47, 379.

96 Y. Hayashi, W. Drawl, R. Messier, *Japn. J. Appl. Phys., Part 2,* **31** (2B) (1992) L193.

97 A.A. Smolin, V.G. Ralchenko, S.M. Pimenov, T.V. Kononenko and others, *Appl. Phys. Lett.,* **62** (26) (1993) 3449.

98 M. Ihara, H. Komiyama and T. Okubo, *Appl. Phys. Lett.,* **65** (9) (1994) 1192.

99 K.F. Turner, B.R. Stoner, L. Bergman, J.T. Glass and others, *J. Appl. Phys.,* **69** (9) (1991) 6400.

100 K. Kobayashi, N. Mutsukura and Y. Machi, *Mater. and Manufacturing Processes*, **7** (3) (1992) 395.

101 Z. Feng, K. Komvopoulos, I.G. Brown and D.B. Bogy, *J. Appl. Phys.*, **74** (4) (1993) 2841.

102 R.A. Rudder, G.C. Hudson, J.B. Posthill, R.E. Thomas and R.J. Marcunas, *Appl. Phys. Lett.*, **59** (1991) 791.

103 S.M. Kanetkar, A.A. Kulkarni, A. Vaidya, R.D. Vispute and others, *Appl. Phys. Lett.*, **63** (6) (1993) 740.

104 J.E. Yehoda, R.I. Fuentes, J.C. Tsang, S.J. Whitehair and others, *Appl. Phys. Lett.*, **60** (23) (1992) 2865.

105 S.J. Lin, S.L. Lee, J. Hwang, C.S. Chang and others, *Appl. Phys. Lett.*, **60** (13) (1992) 1559.

106 J. Narayan, V.P. Godbole, G. Matera and R.K. Singh, *J. Appl. Phys.*, **71** (2) (1992) 966.

107 W.A. Yarbrough, same as Ref. 47, 25.

108 P.A. Dennig, H. Shiomi, D.A. Stevenson and N.M. Johnson,*Thin Solid Films*, **212** (1-2) (1992) 63.

109 J.C. Angus, Y. Wang and M. Sunkara, *Ann. Rev. Mater. Sci.*, **21** (1991) 221.

110 H. Maeda, S. Masuda, K. Kusakabe and S. Morooka, *J. Cryst. Growth*, **121** (3) (1992) 507.

111 M. Yoshikawa, Y. Kaneko, C.F. Yang and H. Tokura, *J. Japan. Soc. Precision Eng.*, **55** (1) (1989) 155.

112 G.F. Zhang, X. Zheng and Z.T. Liu, *J. Cryst. Growth*, **133** (1-2) (1993) 117.

113 S. Yugo, A. Izumi, T. Kanai, T. Muto and T. Kimura, in *New Diamond Sci. Technol.*, MRS Intern. Conf. Proc., Washington DC, Sept. 23 to 27 (1990) 385.

114 N. Ohtake, M. Yoshikawa, K. Suzuki and S. Takeuchi, same as Ref. 47, 431.

115 H. Chen, M.L. Nielsen, C.J. Gold, R.O. Dillon, J. DiGregorio and T. Furtak, same as Ref. 47, 137.

116 M. Yoshikawa, Y. Kaneko, C.F. Yang, H. Tokura and M. Kamo, *J. Japan Soc. Precision Eng.*, **54** (9) (1988) 1703.

117 F. Jansen, M.A. Machonkin and D.E. Kuhman, *J. Vacuum Sci. Technol. A*, **8** (1990) 3785.

118 J.J. Cuomo, J.P. Doyle, D.L. Pappas, K.L. Saenger, C.R. Guarnieri and S.J. Whitehair, same as Ref. 47, 169.

119 R. Beckmann, W. Kulish, H.J. Frenk and R. Kassing, same as Ref. 47, 543.

120 J.L. Valdes, J.W. Mitchel, J.A. Mucha, L. Seibles and H. Huggins, same as Ref. 47, 423.

121 M.W. Geis, *Appl. Phys. Lett.*, **55** (1989) 550; M.W. Geis, A. Argoitia, J.C. Angus, G.-H.M. Ma, J.T. Glass, J. Butler, C.J. Robinson and R. Pryor, *Appl. Phys. Lett.*, **58** (1991) 2485.

122 M. Katoh, M. Aoki and H. Kawarada, *Japn. J. Appl. Phys., Part 2*, **33** (2A) (1994) L194.

123 J.C. Angus and C.C. Hayman, *Science*, **241** (4868) (1988) 913.

124 K. Suzuki, A. Sawabe, H. Yasuda and T. Inuzuka, *Appl. Phys. Lett.*, **50** (12) (1987) 728.

125 R.J. Meilunas, R.P.H. Chang, S. Liu and M.M. Kappes, *Appl. Phys. Lett.*, **59** (26) (1991) 3461.

126 D.E. Meyer, R.O. Dillon and J.A. Woollam, *J. Vacuum Sci. & Technol. A*, **7** (3) (1989) 2325.

127 A.A. Morrish and P.E. Pehrsson, *Appl. Phys. Lett.*, **59** (4) (1991) 417.

128 K. Hirabayashi, Y. Taniguchi, O. Takamatsu, T. Ikeda, K. Ikoma and N.I. Kurihara, *Appl. Phys. Lett.*, **53** (1988) 1815.

129 K. Kobayashi, M. Kumagai, S. Karasawa, T. Watanabe and others, *J. Cryst. Growth*, **128** (1-4) (1993) 408.

130 E. Molinari, R. Polini and M. Tomellini, *J. Mater. Res.*, **8** (4) (1993) 798.

131 K. Kobashi, K. Nishimura, Y. Kawate and T. Horiuchi, *Phys. Rev. B*, **38** (1988) 4067.

132 K. Kobashi, K. Nishimura, K. Miyata, K. Kumagai and A. Nakaui, *J. Mater. Res.*, **5** (11) (1990) 2469.

133 N. Ohtake and M. Yoshikawa, *Japn. J. Appl. Phys., Part 1*, **32** (5A) (1993) 2067.

134 J.C. Angus, R.W. Hoffman and P.H Schmidt, in *Sci. Technol. of New Diamond*, ed. S. Saito, O. Fukunaga and M. Yoshikawa, KTK Terra Scientific, Tokyo, (1990) 9.

135 J.C. Angus, M. Sunkara, S.R. Sahaida and J.T. Glass, *J. Mater. Res.*, **7** (11) (1992) 3001.

136 M. Sunkara, Ph.D. Thesis, Case Western Reserve University (1993).

137 N. Jiang, B.W. Sun, Z. Zhang and Z. Lin, *J. Mater. Res.*, **9** (10) (1994) 2695.

138 M. Frenklach and K.E. Spear, *J. Mater. Res.*, **3** (1988) 133; G.A. Raiche and J.B. Jeffries, *Carbon*, **28** (1990) 796.

139 M. Frenklach and H. Wang, *Phys. Rev.*, **B43** (1991) 1520.

140 A.R. Badzian and R.C. DeVries, *Mater. Res. Soc. Bull.*, **23** (1988) 385; A.R. Badzian, T. Badzian, R. Roy, R. Messier and K.E. Spear, *Mater. Res. Soc. Bull.*, **23** (1988) 531.

141 J.J. Lander and J. Morrison, *Surf. Sci.*, **4** (3) (1966) 241.

142 M. Tomellini, *J. Mater. Res.*, **8** (7) (1993) 1596.

143 P. Badziag, W.S. Verwoerd, W.P. Ellis and N.R. Greiner, *Nature*, **343** (1990) 244.

144 M. Tomellini, R. Polini and V. Sessa, *J. Appl. Phys.*, **70** (12) (1991) 7573; E. Molinari, R. Polini, M.L. Terranova, P. Ascarelli and S. Fontana, *J. Mater. Res.*, **7** (7) (1992) 1778.

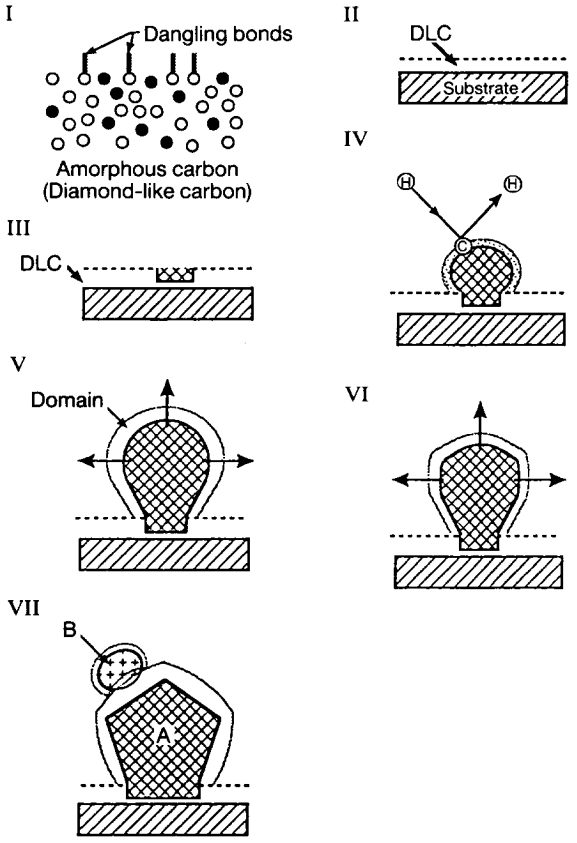

Figure 1 Schematic showing the proposed nucleation mechanism: diamond nuclei form on a DLC interlayer. I: formation of carbon clusters on substrate surface and change in bonding structure from sp^1 to sp^2; II: conversion of sp^1->sp^2->sp^3 bonding; III: crystallization of amorphous phase; IV-VI: growth and faceting of diamond crystal; VII: secondary nucleation and growth of diamond [9].

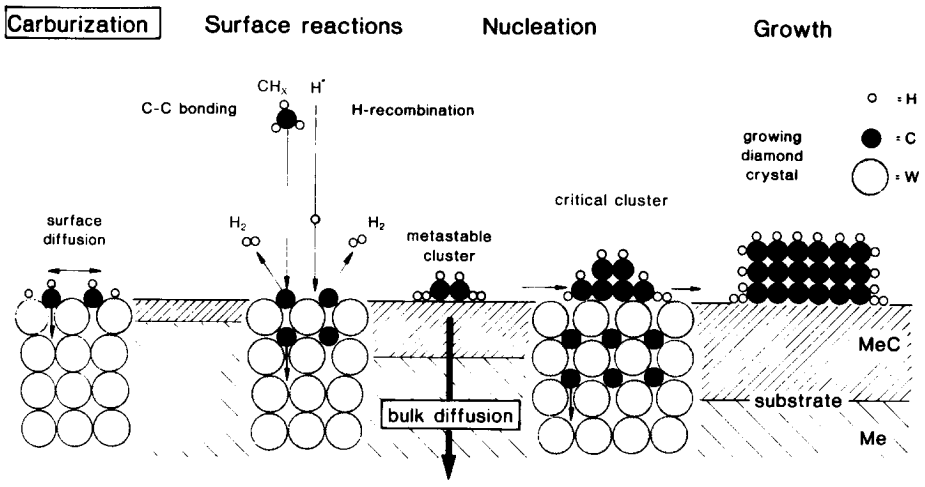

Figure 2 Schematic showing the proposed nucleation mechanism: diamond nuclei form on a carbide interlayer on a carbide-forming refractory metal substrate [72]. Initially, carburization consumes all available C to form a carbide surface layer. A minimum C surface concentration required for diamond nucleation cannot be reached on the substrate surface. With increasing carbide layer thickness, the C transport rate slows and the C surface concentration increases. When the C surface concentration reaches a critical level for diamond nucleation, or a surface C cluster attains a critical size, a diamond nucleus forms.

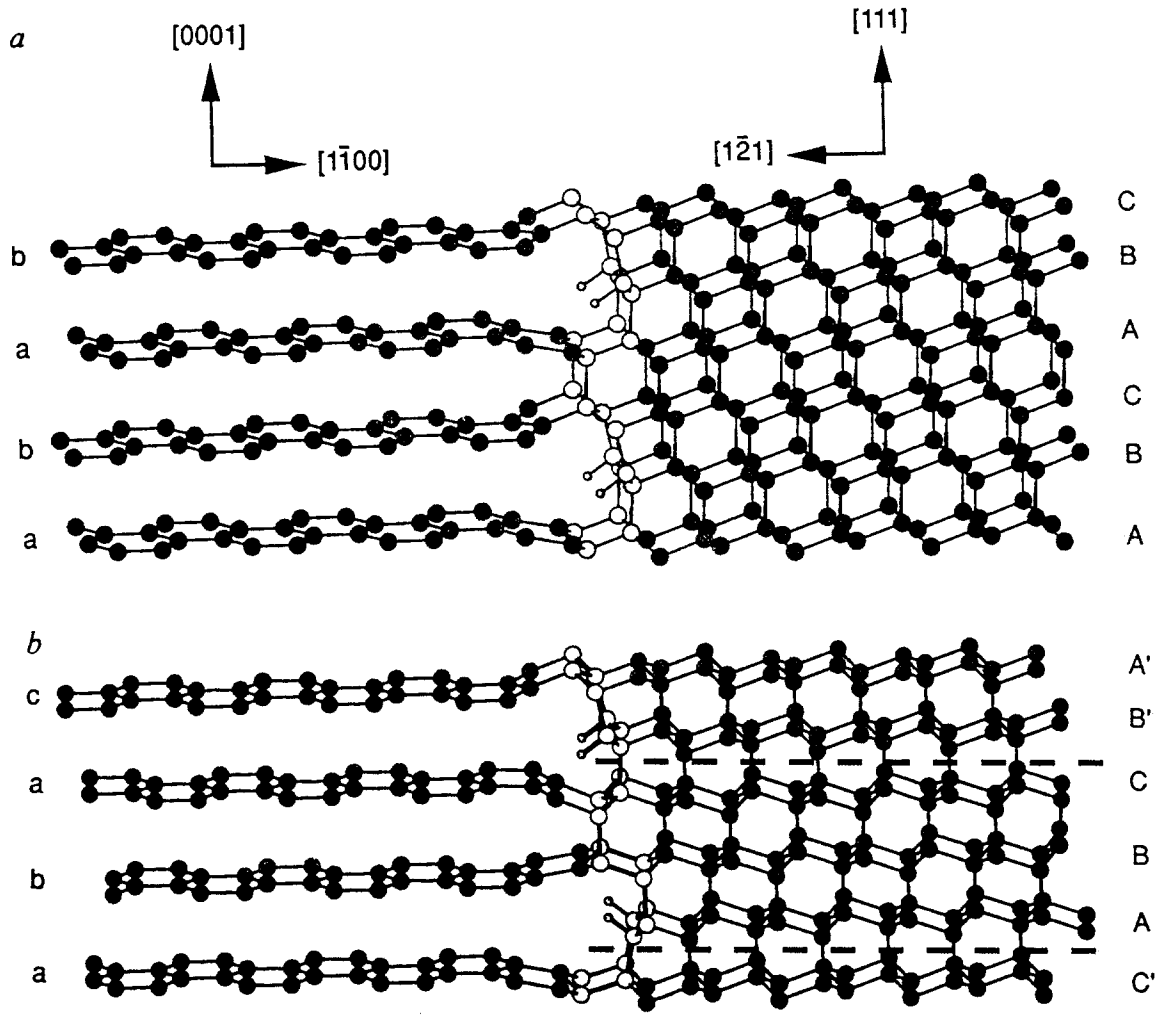

Figure 3 Schematic showing the proposed nucleation mechanism: diamond nuclei form on a graphite interlayer [13]. Initial condensation of graphite and subsequent hydrogenation of the $\{1\bar{1}00\}$ prism planes along the edges of graphite particles are followed by kinetically preferential nucleation of diamond at the emerging graphite stacking faults, and with an almost perfect interface between the graphite layer and the diamond nuclei. Upper: cubic diamond on perfect hexagonal graphite; Lower: a twinned diamond nucleus adjoining a graphite stacking fault. Twin boundaries in diamond are indicated by the dashed lines, H atoms by the small open circles, and C atoms by dark solid circles. The larger open circles indicate the initial nucleus formed at the interface by tying together the graphite layer with tetrahedrally bonded C atoms.

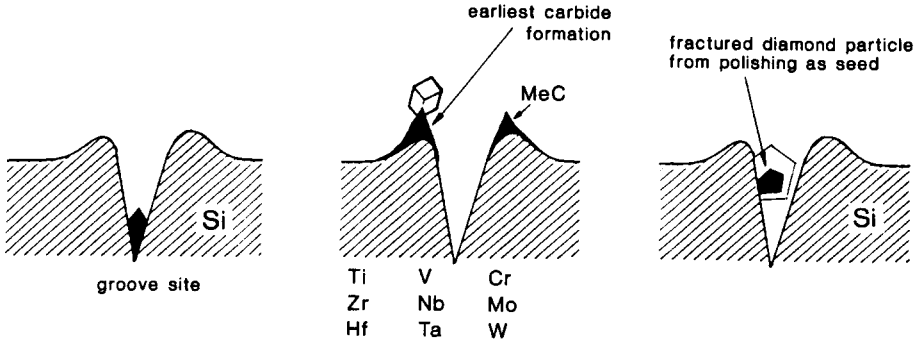

Figure 4 Schematic diagram of mechanisms for diamond nucleation enhancement on scratched substrates [72].

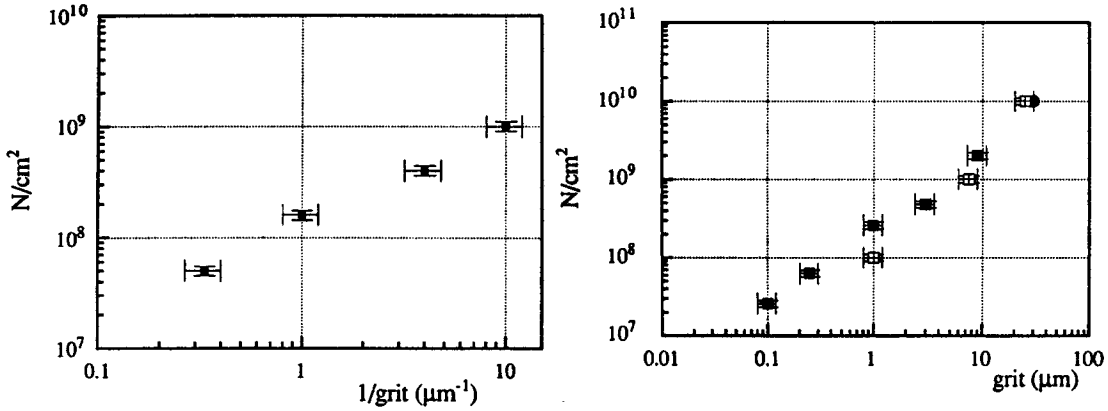

Figure 5 Dissimilar grit-size dependence of diamond nucleation density on substrate surface pretreatments. (a) Nucleation density versus inverse abrasive paste mean-size used in polishing pretreatment; (b) Nucleation density versus single-particle mean-size used in ultrasonic pretreatment [39].

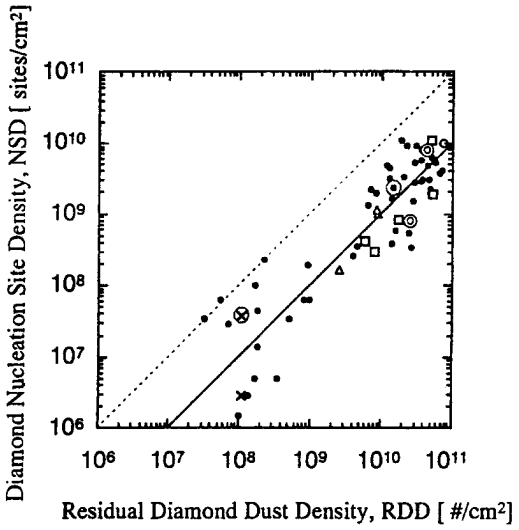

Figure 6 Dependence of diamond nucleation site density (NSD) on residual diamond particle density (RDD) under various deposition conditions. The dotted line shows NSD equal to RDD and the solid line shows NSD being 10% of RDD. Solid circles: ultrasonic polishing, followed by MW PACVD, Crosses: hand polishing, followed by MW PACVD, triangles: ultrasonic polishing, followed by HFCVD (filament temperature=2973K), squares: ultrasonic polishing, followed by HFCVD (filament temperature=2773K), open circles: ultrasonic polishing, followed by HFCVD (filament temperature=2573K), dotted circles: fluidized-diamond polishing, followed by MW PACVD [98].

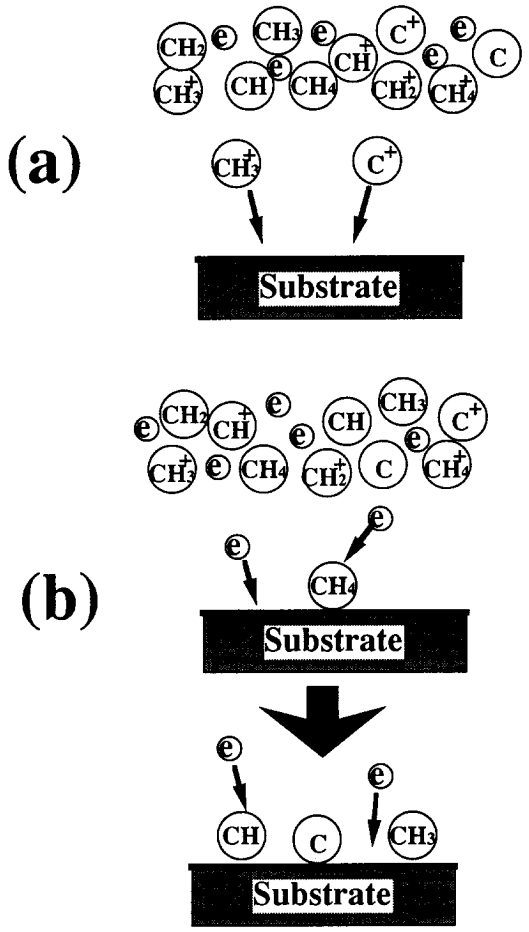

Figure 7 Schematic diagram of mechanisms for diamond nucleation enhancement on biased substrates. (a) negative bias: carbon-containing cations are accelerated toward the substrate surface; (b) positive bias: electrons are accelerated toward the substrate surface and bombard carbon-containing molecules adsorbed on the surface [122].

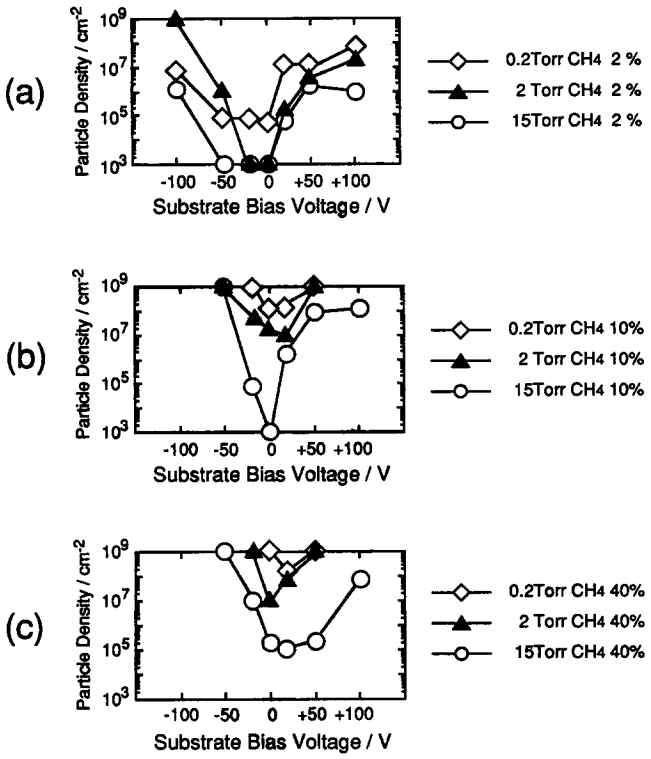

Figure 8 Diamond particle density as a function of substrate bias voltage, gas pressure and CH_4 concentration. In bias pretreatments, substrate bias voltage ranges from -100 V to +100 V, gas pressure varies from 0.2, 2 to 15 torr and CH_4 concentration from 2 (a), 10 (b) to 40 % (c) [122].

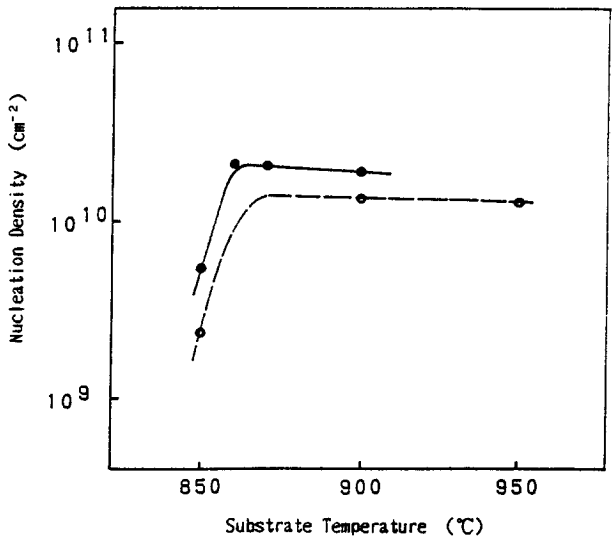

Figure 9 Temperature dependence of diamond nucleation density measured by ellipsometric monitor. Solid circles and solid line show values for 1000 W microwave power; open circles and dash line show values for 1400 W microwave power. Other deposition conditions: 5%CO/H_2, flow rate of 100 sccm, and pressure of 50 torr. Using CO as reactive gas led to diamond films containing hardly any non-diamond phases [96].